AIP | The Journal of Chemical Physics

Local ab initio methods for calculating optical bandgaps in periodic systems. II. Periodic density fitted local configuration interaction singles method for solids

Marco Lorenz, Lorenzo Maschio, Martin Schütz, and Denis Usvyat

Citation: The Journal of Chemical Physics **137**, 204119 (2012); doi: 10.1063/1.4767775
View online: http://dx.doi.org/10.1063/1.4767775
View Table of Contents: http://scitation.aip.org/content/aip/journal/jcp/137/20?ver=pdfcov
Published by the AIP Publishing

Local *ab initio* methods for calculating optical bandgaps in periodic systems. II. Periodic density fitted local configuration interaction singles method for solids

Marco Lorenz,[1] Lorenzo Maschio,[2] Martin Schütz,[1,a)] and Denis Usvyat[1,b)]
[1]*Institute for Physical and Theoretical Chemistry, Universität Regensburg, Universitätsstrasse 31, D-93040 Regensburg, Germany*
[2]*Dipartimento di Chimica, and Centre of Excellence NIS (Nanostructured Interfaces and Surfaces), Università di Torino, via Giuria 5, I-10125 Torino, Italy*

(Received 30 July 2012; accepted 2 November 2012; published online 29 November 2012)

We present a density fitted local configuration interaction singles (CIS) method for calculating optical bandgaps in 3D-periodic systems. We employ an Ewald technique to carry out infinite lattice summations for the exciton-exciton interaction, and robust product-density specific local density fitting in direct space for the electron-hole interaction. Moreover, we propose an alternative to the usual cyclic model with Born-von Karman periodic boundary conditions, the so called Wigner-Seitz supercell truncated infinite model, which exhibits much improved convergence of the CIS excitation energy with respect to the size of the supercell. Test calculations on a series of prototypical systems demonstrate that the method at the present stage can be used to calculate the excitonic bandgaps of 3D periodic systems with up to a dozen atoms in the unit cell, ranging from wide-gap insulators to semiconductors. © *2012 American Institute of Physics*. [http://dx.doi.org/10.1063/1.4767775]

I. INTRODUCTION

Although the electronic bandgap is one of the most important characteristic properties of crystalline systems, its rigorous theoretical description is difficult. Time-dependent density functional theory (TD-DFT), which is one of the most common techniques in molecular excited state studies, is hardly applicable for periodic systems. One of the intrinsic problems of DFT, the self-interaction error, artificially lowers the excitation energies of excited states with charge transfer character. In infinite systems, this has extreme consequences: the lowest non-hybrid TD-DFT excitation energy is equal to the simple DFT highest occupied crystalline orbital (HOCO) - lowest unoccupied crystalline orbital (LUCO) energy difference.[1,2] An approach to excited states in periodic systems, based on the quasi-energy GW formalism,[3,4] is more successful. It provides a first-order correction to the Kohn-Sham orbital energies, and, if furthermore combined with solving the quasi-particle Bethe-Salpeter equation, includes the excitonic effects, i.e., the electron-hole attraction.[4–10] Calculations employing these methods are, however, computationally rather expensive.

The quantum chemical approach to the problem, i.e., starting from a configuration interaction singles (CIS) wavefunction and subsequently including correlation effects, which has been very successfully applied in countless molecular studies, is to a large extent unexplored for solids. Previous work in this context includes 1D periodic implementations of the uncorrelated CIS method,[1] and correlation corrections to it.[11,12] There are also examples of early applications of approximate CIS or time-dependent Hartree-Fock (TD-HF) techniques to simple 3D systems.[1] Recently, also a 3D periodic semiempirical CIS implementation, based on the intermediate neglect of differential overlap approximation, has been reported.[13] There exists also a periodic implementation of the algebraic diagrammatic construction scheme for the self-energy in the canonical representation.[14] An alternative technique to evaluate the TD-HF excitation energies in periodic systems has been developed in Ref. 15. It implies fitting of the explicitly calculated values of the coupled perturbed HF polarizability to a model function, inversely dependent on frequency. The excitation energies are then evaluated as poles of this model function.

Finally, finite cluster approaches to excited states of periodic systems, based on the incremental scheme,[16] or other fragment techniques, have been proposed.[17–19] However, the slow convergence with cluster size (depending on the character of the excited state) and the existence of parasitic cluster surface states render such approaches as not straightforward.

The goal of our work is to develop a hierarchy of periodic quantum chemical excited state methods for solids. In a previous paper[20] (denoted in the following as Paper I), we have presented formalism, implementation, and test applications of a periodic local density fitted CIS method for 1D periodic systems like polymers. In the present work, the second paper in this series, the method is generalized to full 3D periodic systems (crystals). There are two fundamental complications compared to the 1D case. First, the infinite lattice sums occurring in the Coulomb part of the matrix-vector product[20] no longer converge. Second, the direct space density fitting approach based on a single common fit-domain, as employed in the 1D case to calculate the exchange part of the matrix-vector product becomes prohibitively expensive for bulky systems. To remedy the first problem, the Coulomb part is now calculated by employing an approach based on

a)Electronic mail: martin.schuetz@chemie.uni-regensburg.de.
b)Electronic mail: denis.usvyat@chemie.uni-regensburg.de.

an approximate Ewald potential function,[21] using multipole representations of the periodically repeated product densities beyond a certain distance. To fix the second problem a product-density specific local density fitting scheme in direct space with multiple different fit-domains is now used for the exchange part. In order for the fit to be robust, i.e., to make the fitting error in the integrals second-order with respect to the fitting error in the individual orbital product densities, the three-term formula for density fitting has to be used.

The paper is organized as follows: in Sec. II, we briefly review the theory for periodic local CIS, and discuss the cyclic, and the Wigner-Seitz supercell truncated infinite models (WSS-TIM). Then, the calculation of the Coulomb and exchange parts of the matrix-vector product via Ewald, and local density fitting in direct space, respectively, are discussed. In Sec. III, we briefly focus on some details of the implementation, relevant for accuracy and computational efficiency. In Sec. IV, we present results from test calculations for different crystals, ranging from wide-gap insulators to semiconductors. The focus here is on the locality of the exciton in reciprocal and direct space. Section V finally concludes the paper.

II. PERIODIC LOCAL CIS THEORY

In the present paper, we use the same convention for indices as in Paper I: indices $i, j, \ldots$ and $a, b, \ldots$ denote Wannier functions (WFs)[22,23] ϕ_i, ϕ_j, $\ldots$ and projected atomic orbitals (PAOs)[20,24–26] ϕ_a, ϕ_b, $\ldots$, respectively, or their Fourier images. WFs and PAOs are local orbitals spanning the occupied and virtual spaces, respectively. For the corresponding canonical orbitals indices with an overbar are used. Indices P, Q, $\ldots$ denote auxiliary fitting functions ϕ_P, ϕ_Q, $\ldots$ and μ, ν, $\ldots$ AOs ϕ_μ, ϕ_ν, $\ldots$. The calligraphic indices $\mathcal{I}$, $\mathcal{A}$, $\mathcal{P}$, $\mathcal{M}$, $\ldots$ identify the lattice vectors $\mathbf{R}_\mathcal{I}$, $\mathbf{R}_\mathcal{A}$, $\mathbf{R}_\mathcal{P}$, $\mathbf{R}_\mathcal{M}$, $\ldots$ of the cells, where the functions $\phi_{i\mathcal{I}}$, $\phi_{a\mathcal{A}}$, $\phi_{P\mathcal{P}}$, $\phi_{\mu\mathcal{M}}$, $\ldots$, respectively, are centered. Sums or differences between lattice vectors are denoted by $\oplus$ and $\ominus$ symbols, respectively, applied to the corresponding cell indices. Products of two orbitals are called product densities and designated by the symbol ρ, e.g., $\rho_{\mu\nu\mathcal{N}} = \phi_\mu\phi_{\nu\mathcal{N}}$. The atoms, the PAOs ϕ_a, ϕ_b, $\ldots$ belong to, are denoted as A, B, $\ldots$. Vectors $\mathbf{k}_i$, $\mathbf{k}_a$, and $\mathbf{k}_P$ are the wavevectors of the first Brillouin zone (BZ) (i.e., the so called **k**-vectors or **k**-points) corresponding to the occupied, virtual, or auxiliary functions. The chemical (Mulliken) notation is employed for the two-electron integrals.

The CIS wavefunction for a Γ-point exciton, as introduced in Paper I, reads

$$\Psi^\Gamma_{\text{exc}} = \sum_{ia\mathcal{A}} c^i_{a\mathcal{A}} \sum_{\mathcal{I}} \Phi^{a(\mathcal{A}+\mathcal{I})}_{i\mathcal{I}} = \sum_{\bar{i}\bar{a}\mathbf{k}} c^{\bar{i}}_{\bar{a}}(\mathbf{k})\Phi^{\bar{a}}_{\bar{i}}(\mathbf{k}), \qquad (1)$$

where **k** is the translational symmetry index of both the occupied and virtual canonical orbitals $\bar{i}$ and $\bar{a}$ (for the Γ-point excitons they have to coincide (cf., Eq. (6) in Ref. 20). $\Phi^{a(\mathcal{A}+\mathcal{I})}_{i\mathcal{I}}$ and $\Phi^{\bar{a}}_{\bar{i}}(\mathbf{k})$ are singly excited determinants in local and canonical space, respectively.

The CIS eigenvalue problem is solved by means of the Davidson diagonalization procedure,[27] carried out in the canonical (reciprocal) space. The refresh procedure is used for the small Davidson subspace not to exceed a predefined maximal size. The standard first-order update for the trial vector,

$$(\Delta\mathbf{c}^{(n)})^{\bar{i}}_{\bar{a}}(\mathbf{k}) = -\frac{(\mathbf{Hc}^{(n)})^{\bar{a}}_{\bar{i}}(\mathbf{k}) - \omega^{(n)}_{\text{CIS}}(\mathbf{c}^{(n)})^{\bar{i}}_{\bar{a}}(\mathbf{k})}{\varepsilon_{\bar{a}}(\mathbf{k}) - \varepsilon_{\bar{i}}(\mathbf{k}) - \omega^{(n)}_{\text{CIS}}}, \qquad (2)$$

is used, with a subsequent orthogonalization to the previous-iteration trial vectors of the small Davidson space and normalization. Here, **H** stands for the CIS Hamiltonian, $\mathbf{c}^{(n)}$ and $\omega^{(n)}_{\text{CIS}}$ are the nth iteration CIS vector and excitation energy, respectively, and the orbital energies at a certain **k**-point are denoted by $\varepsilon_{\bar{i}}(\mathbf{k})$ and $\varepsilon_{\bar{a}}(\mathbf{k})$.

The matrix-vector products $(\mathbf{Hc})^{\bar{a}}_{\bar{i}}(\mathbf{k})$ required to evaluate the small Davidson space Hamiltonian matrix (Eq. (12) in Ref. 20) and the residuum (here, **c** stands for a trial or full CIS vector) are partially calculated in canonical and partially in local space,

$$\begin{aligned}(\mathbf{Hc})^{\bar{a}}_{\bar{i}}(\mathbf{k}) =& \big(\varepsilon_{\bar{a}}(\mathbf{k}) - \varepsilon_{\bar{i}}(\mathbf{k})\big)c^{\bar{i}}_{\bar{a}}(\mathbf{k}) \\ &+ \mathcal{FT}_{\mathbf{R}_\mathcal{A}}\Big\{2\sum_{j\mathcal{J}b\mathcal{B}}(i\ a\mathcal{A}|j\mathcal{J}\ b\mathcal{B})c^{j\mathcal{J}}_{b\mathcal{B}} \\ &- \sum_{j\mathcal{J}b\mathcal{B}}(i\ j\mathcal{J}|a\mathcal{A}\ b\mathcal{B})c^{j\mathcal{J}}_{b\mathcal{B}}\Big\}, \end{aligned} \qquad (3)$$

where $\mathcal{FT}_{\mathbf{R}_\mathcal{A}}$ denotes the Fourier transformation with respect to the vector $\mathbf{R}_\mathcal{A}$.

The two-electron part **Vc** of the CIS matrix-vector product $\mathbf{Hc} = \mathbf{Fc} + \mathbf{Vc}$ consists of the so called Coulomb term (which describes the exciton-exciton interaction and vanishes for a triplet state)

$$({}^{\text{coul}}\mathbf{Vc})^{a\mathcal{A}}_i = \sum_{j\mathcal{J}b\mathcal{B}}(i\ a\mathcal{A}|j\mathcal{J}\ b\mathcal{B})c^{j\mathcal{J}}_{b\mathcal{B}} \qquad (4)$$

and the exchange term (which describes the electron-hole attraction)

$$({}^{\text{exch}}\mathbf{Vc})^{a\mathcal{A}}_i = \sum_{j\mathcal{J}b\mathcal{B}}(i\ j\mathcal{J}|a\mathcal{A}\ b\mathcal{B})c^{j\mathcal{J}}_{b\mathcal{B}}. \qquad (5)$$

These contractions are calculated with robust density fitting, which factorizes the four-index electron repulsion integrals (ERIs) into three- and two-index objects.[28–35] Different decay behaviour of the lattice summations in Eqs. (4) and (5) lead to two principally different density fitting approaches. The Coulomb term Eq. (4), involving long-range summations, is fitted in the reciprocal space, while the relatively short-range exchange term Eq. (5) (governed by the locality of the exciton) is fitted in the direct space (*vide infra*).[20]

A. Cyclic model versus Wigner-Seitz supercell truncated infinite model of a crystal

The cell index $\mathcal{A}$ in the direct representation of the CIS coefficients $c^i_{a\mathcal{A}}$ in Eq. (1) or the matrix-vector products $(\mathbf{Vc})^{a\mathcal{A}}_i$ in Eq. (4) or (5) formally runs to infinity. For obvious reasons, however, it is not possible to treat a crystal as an infinite object in practical calculations. Fortunately, locality of the exciton can effectively truncate the essential range for this index, which does not need to extend further than the exciton to be captured.

In Paper I, a cyclic model for a crystal, i.e., a finite model with Born-von Karman periodic boundary conditions, was considered. Such a model features a finite number of **k**-points in the reciprocal space representation of the wavefunction (1), equal to the number of unit cells $\mathcal{A}$ in the supercell of the cyclic system.[20,36,37] The transformations between the direct and reciprocal spaces correspond in this case to the discrete Fourier and inverse-Fourier transforms [e.g., in Eq. (3)]. The convergence of the excitation energies with respect to the supercell size was explored in Paper I by increasing the supercell size, and, with that, the density of the **k**-mesh.

Yet, in the infinite model of a crystal the direct space representation of, e.g., the CIS-coefficients are, in fact, the coefficients of an infinite Fourier-series expansion of the reciprocal space CIS-coefficients $c_a^i(\mathbf{k})$. For fixed i and a the latter is a continuous and periodic function of the variable **k**,

$$c_a^i(\mathbf{k}) = \sum_{\mathcal{A}} c_{a\mathcal{A}}^i \exp(\imath \mathbf{k} \cdot \mathbf{R}_{\mathcal{A}}). \tag{6}$$

The Fourier-coefficients $c_{a\mathcal{A}}^i$ in turn are defined as integrals over the period in the **k**-space, i.e., the BZ,

$$c_{a\mathcal{A}}^i = \int_{\mathrm{BZ}} \mathrm{d}\mathbf{k} c_a^i(\mathbf{k}) \exp(-\imath \mathbf{k} \cdot \mathbf{R}_{\mathcal{A}}). \tag{7}$$

The same holds for the matrix-vector products $(\mathbf{Vc})_i^a(\mathbf{k})$.

Starting from this model, an approximation can be introduced in Eq. (6), which restricts the number of the terms in the Fourier series, without affecting the expression for the Fourier coefficients (7). In practice, of course, the integration (7) has to be performed numerically using a large, but finite number of **k**-points. But importantly, the density of the **k**-mesh, used for the integral quadrature, is now effectively decoupled from the number of the direct space vectors used in the finite summation (6). The truncation of the Fourier series is done in our approach by restricting the index $\mathcal{A}$ to a supercell, chosen in the WS form. For each CIS coefficient $c_{a\mathcal{A}}^i$ or matrix-vector product $(\mathbf{Vc})_i^{a\mathcal{A}}$, the origin of the WS supercell is chosen to coincide with the centering point of the WF ϕ_i. With this definition the most rapid convergence of the truncated Fourier series to the untruncated result is expected, since for each i the truncating surface, i.e., the border of the Wigner-Seitz supercell, is as distant and as spherical-like as possible. Furthermore, since the Wigner-Seitz supercell is invariant with respect to the point group symmetry of the crystal, the symmetry of the exciton is not compromised by the truncation. For future reference, we denote this model as the WSS-TIM model of a crystal as an alternative to the cyclic model.

For the CIS method for polymers reported in Paper I very large supercells could be used without a considerable penalty in the computational time. Therefore, the number of unit cells in the supercell was set to be equal to the number of **k**-vectors in the mesh, i.e., the cyclic model was always employed. In bulky systems, however, the situation is different. Expansion of a 3D supercell is very costly due to the cubic increase of the number of unit cells (and the ERIs to be computed) with linear increase in the supercell size. Therefore, in our approach, where the computational demands for the reciprocal space part of the calculation [Eqs. (2) and (3)] are negligible compared to that of the direct space (*vide infra*), at least for small and medium sized unit cells, WSS-TIM is clearly advantageous.

From the angle of WSS-TIM, the cyclic model for not yet converged results suffers from two independent sources of errors (i) the inaccurate quadrature for the **k**-point integration (7), and (ii) the truncation of the Fourier series (6). The integration over the BZ (7) in our case can be performed very accurately, employing very dense **k**-meshes, and hence, eliminating one (and, as the calculations show, cf. Sec. IV C, the main) of these two deficiencies. This substantially speeds up the convergence of the results with respect to the $\mathcal{A}$-truncation range, which in WSS-TIM is the only remaining approximation.

B. Density fitting for the Coulomb term

As was shown in Ref. 20, evaluation of the Coulomb term Eq. (4) simplifies considerably within the reciprocal-space density fitting procedure. The orthogonality relations for the irreps of the translational symmetry group (represented by the **k**-vectors) eliminate all but the $\mathbf{k}_P = 0$ term from the $\mathbf{k}_P$-summation (integration) of the back-Fourier transform,[20,34,38] yielding

$$({}^{\mathrm{coul}}\mathbf{Vc})_i^{a\mathcal{A}} = \sum_P (i\ a\mathcal{A}|P)^*_{(\mathbf{k}_P=0)} \sum_{j\ b\mathcal{B}'} d^{j\ b\mathcal{B}'}_{P(\mathbf{k}_P=0)} c^j_{b\mathcal{B}'}, \tag{8}$$

where $(i\ a\mathcal{A}|P)_{(\mathbf{k}_P)}$ and $d^{j\ b\mathcal{B}'}_{P(\mathbf{k}_P)}$ are the Fourier images of the three-index Coulomb integrals and density fitting coefficients, respectively, and the vector $\mathcal{B}'$ is defined as $\mathcal{B} \ominus \mathcal{J}$. The DF coefficients, which correspond to the minimum of the fitting functional with the Coulomb metric, are evaluated also in the reciprocal space[20] as

$$d^{j\ b\mathcal{B}'}_{P(\mathbf{k}_P)} = \sum_Q (j\ b\mathcal{B}'|Q)_{(\mathbf{k}_P)} ([J_{(\mathbf{k}_P)}]^{-1})_{QP}, \tag{9}$$

whereas the three-index integrals are calculated in the direct space and Fourier-transformed thereafter,

$$(i\ a\mathcal{A}|P)_{(\mathbf{k}_P=0)} = \sum_{\mathcal{P}} (i\ a\mathcal{A}|P\mathcal{P}). \tag{10}$$

The same applies also to the two-index metric matrix, the inverse of which is occurring in Eq. (9); it is the reciprocal image of the two-index Coulomb integral,

$$(J_{(\mathbf{k}_P=0)})_{QP} = (Q|P)_{(\mathbf{k}_P=0)} = \sum_{\mathcal{P}} (Q|P\mathcal{P}). \tag{11}$$

As seen from Eqs. (10) and (11), evaluation of both the three-index $(i\ a\mathcal{A}|P)_{(\mathbf{k}_P=0)}$ and two-index $(Q|P)_{(\mathbf{k}_P=0)}$ reciprocal images of the Coulomb integrals imply non-convergent infinite lattice summations in the 3D case. This non-convergence issue is not a feature of the reciprocal space density fitting formalism, but reflects the true physics of the Coulomb CIS term (4), which indeed is of long-range nature.

Due to the mutual orthogonality of the occupied and virtual spaces, the interacting $ia\mathcal{A}$-product densities are chargeless. This guarantees that the lattice sum (4) of the Coulomb term is convergent, although only conditionally. s-type fitting functions, on the other hand, are not chargeless, which would lead to divergent summations (10) and (11). A remedy to

this problem is the use of mixed auxiliary basis sets, containing Poisson-type-orbitals (PTOs), together with a few GTOs. The use of PTOs as a fitting basis[35,39–41] allows for a stable scheme, which does not involve any charge-multipole interactions. The PTOs, which are Laplacians of standard GTOs, are free of moments of any order. This property leads to an exponential decay of the Coulomb integrals, and therefore to a fast decay of the lattice sums (10) and (11). PTOs, however, must be complemented by a few GTOs in order to fully represent real product densities, which are not momentless. It is, in fact, sufficient to introduce just one GTO of each angular momentum per center. Since, as discussed above, $ia\mathcal{A}$-product densities are chargeless, the troublesome s-type GTOs are not needed.

The convergence of the lattice sums involving GTO-fitting functions (especially the p-GTOs) in 3D still remains an issue. Note that the use of a combined PTO-GTO fitting basis implies that for the main PTO-part of the fitting basis the lattice sums (10) and (11) converge exponentially.[42] Nevertheless, for the smaller GTO-part of the fitting basis the summations (10) and (11) converge either very slowly or even only conditionally and thus convergence acceleration techniques like the Ewald procedure are needed.

The value, to which a conditionally convergent series converges, depends on the chosen order of summation. For Coulomb lattice sums, this mathematical uncertainty in an infinite lattice reflects the strong dependence of the electrostatic potential on the particular shape of a real finite crystal. The Ewald-type summation of the conditionally convergent series effectively corresponds to a specific choice of the summation order, each partial sum of which corresponds to zeroing the charge, dipole, and quadrupole moments of the unit cell, canceling thus the not absolutely convergent contributions.[43] Formally, this is equivalent to a substitution of the conditionally convergent Coulomb potential [Eq. (18) of Ref. 21] by an Ewald potential [Eqs. (43) and (44) of Ref. 21], which consists of two absolutely convergent sums. The Ewald technique dates back to more than 90 years,[44] and different formulations of it have been proposed over the years.[43] Here, we adopt an implementation used in the CRYSTAL program to compute the Coulomb part of the Fock matrix in HF or DFT calculations.[21,45]

In the present context, the Ewald procedure is utilized for calculating the three-index integrals in the AO basis,

$$(\mu\nu\mathcal{N}|P)_{(\mathbf{k}_P=0)} = \sum_{\mathcal{P}}(\mu\nu\mathcal{N}|P\mathcal{P}) = \sum_{\mathcal{P}}(\mu(\ominus\mathcal{P})\nu(\mathcal{N}\ominus\mathcal{P})|P). \quad (12)$$

Evaluation of such an integral proceeds via three quantities,

$$(\mu\nu\mathcal{N}|P)_{(\mathbf{k}_P=0)} = {}^{\mathrm{Ew}}\Theta^{P}_{\mu\nu\mathcal{N}} - \delta\Theta^{P}_{\mu\nu\mathcal{N}}(\{\mathcal{P}\}_{\mathrm{pen}}) + \delta K^{P}_{\mu\nu\mathcal{N}}(\{\mathcal{P}\}_{\mathrm{pen}}), \quad (13)$$

which are defined in the following.

The first term ${}^{\mathrm{Ew}}\Theta^{P}_{\mu\nu\mathcal{N}}$ is the contribution originating from the Ewald potential

$${}^{\mathrm{Ew}}\Phi_{\mu\nu\mathcal{N}}(\mathbf{r}) = \int \mathrm{d}\mathbf{r}'\rho_{\mu\nu\mathcal{N}}(\mathbf{r}')A(\mathbf{r}'-\mathbf{r}), \quad (14)$$

of an infinite lattice, generated by the periodic images of the AO product densities $\rho_{\mu\nu\mathcal{N}}$. Here, $A(\mathbf{r})$ is the Ewald potential function, defined in Eq. (44) of Ref. 21, which consists of two absolutely convergent series, one with respect to the direct space vectors, the other with respect to the reciprocal space vectors. The interaction between the lattice of the periodically repeated densities $\rho_{\mu\nu\mathcal{N}}$ and the fitting function ϕ_P is evaluated by invoking the multipole representation of the latter with the multipole moments η^{ml}_P of the angular momentum l and its projection m,

$${}^{\mathrm{Ew}}\Theta^{P}_{\mu\nu\mathcal{N}} = {}^{\mathrm{Ew}}\Phi_{\mu\nu\mathcal{N}}(\mathbf{r}_P)\sum_{l=0}^{l_{max}}\sum_{m=-l}^{l} Z^{ml}(\mathbf{r}_P)\eta^{ml}_P(\mathbf{r}_P). \quad (15)$$

Here, $\mathbf{r}_P$ is the position vector of the center of the fitting function ϕ_P, and $Z^{ml}(\mathbf{r})$ denotes the renormalized solid harmonics, corresponding to the angular momentum l and m (Eqs. (97) and (98) of Ref. 21). The expression (15) utilizes the fact that the fitting GTOs do not possess charge (*vide supra*), and thus their spheropole[21] is zero.

The second and third terms of (13) provide a correction to the Ewald potential in the region around the fitting function ϕ_P, where it overlaps with the (periodically repeated) densities $\rho_{\mu\nu\mathcal{N}}$, rendering the multipole representation of the former as invalid. This region (or cavity) is determined on the basis of the overlap between the most diffuse Gaussians of $\phi_{\mu(\ominus\mathcal{P})}$, $\phi_{\nu(\mathcal{N}\ominus\mathcal{P})}$, and ϕ_P as a subset $\{\mathcal{P}\}_{\mathrm{pen}}$ of $\mathcal{P}$-vectors. The densities $\rho_{\mu(\ominus\mathcal{P})\nu(\mathcal{N}\ominus\mathcal{P})}$ with $\mathcal{P}\in\{\mathcal{P}\}_{\mathrm{pen}}$ hence can significantly penetrate the fitting functions ϕ_P. By default, a threshold of 10^{-9} is used for the overlap criterion defining this cavity. The quantities $\delta\Theta^{P}_{\mu\nu\mathcal{N}}(\{\mathcal{P}\}_{\mathrm{pen}})$ and $\delta K^{P}_{\mu\nu\mathcal{N}}(\{\mathcal{P}\}_{\mathrm{pen}})$ are calculated within this cavity as

$$\delta\Theta^{P}_{\mu\nu\mathcal{N}}(\{\mathcal{P}\}_{\mathrm{pen}}) = \sum_{\mathcal{P}\in\{\mathcal{P}\}_{\mathrm{pen}}}\left[\int \mathrm{d}\mathbf{r}\frac{\rho_{\mu\nu\mathcal{N}}(\mathbf{r})}{|\mathbf{r}-\mathbf{R}_{\mathcal{P}}-\mathbf{r}_P|}\right] \times \sum_{l=0}^{l_{max}}\sum_{m=-l}^{l} Z^{ml}(\mathbf{r}_P)\eta^{ml}_P(\mathbf{r}_P), \quad (16)$$

and

$$\delta K^{P}_{\mu\nu\mathcal{N}}(\{\mathcal{P}\}_{\mathrm{pen}}) = \sum_{\mathcal{P}\in\{\mathcal{P}\}_{\mathrm{pen}}}(\mu(\ominus\mathcal{P})\nu(\mathcal{N}\ominus\mathcal{P})|P) = \sum_{\mathcal{P}\in\{\mathcal{P}\}_{\mathrm{pen}}}(\mu\nu\mathcal{N}|P\mathcal{P}). \quad (17)$$

The term (16) subtracts from the integral (15) the contribution from the cavity $\{\mathcal{P}\}_{\mathrm{pen}}$, treated at the point-multipole level. This contribution is then recalculated explicitly in (17), i.e., without the multipole approximation, and added to the integral $(\mu\nu\mathcal{N}|P)_{(\mathbf{k}_P=0)}$.

After calculating the three-index integrals (12) in AO basis they are transformed to WF/PAO basis, yielding the transformed three-index integrals of Eq. (10), as required in

Eq. (8),

$$(ia\mathcal{A}|P)_{(\mathbf{k}_P=0)} = \sum_{\nu\mathcal{N}} C_{\nu(\mathcal{N}\ominus\mathcal{A}),a} \sum_{\mu\mathcal{M}} C_{\mu\mathcal{M},i} \times (\mu\nu(\mathcal{N}\ominus\mathcal{M})|P)_{(\mathbf{k}_P=0)}. \quad (18)$$

Here, $C_{\nu(\mathcal{N}\ominus\mathcal{A}),a} = C_{\nu\mathcal{N},a\mathcal{A}}$ and $C_{\mu\mathcal{M},i}$ are the LCAO coefficients of the WF ϕ_i, and the PAO $\phi_{a\mathcal{A}}$, respectively.

The two-index integrals (11) are treated analogously, with the sole difference that instead of the orbital product density $\rho_{\mu\nu\mathcal{N}}$ an auxiliary function ϕ_Q enters, and an AO to MO transformation (18) is obviously not needed. To evaluate the objects ${}^{\mathrm{Ew}}\Theta^P_{\mu\nu\mathcal{N}}$ and $\delta\Theta^P_{\mu\nu\mathcal{N}}(\{\mathcal{P}\}_{\mathrm{pen}})$ already existing CRYSTAL routines, adapted for the current purpose, are employed.[21,46]

C. Density fitting for the exchange term

The ERIs occurring in the Coulomb (4) and exchange (5) terms are different. In the latter, the orbital product distributions of the ERIs generally are not chargeless. This, in turn, requires s-type GTOs to be included in the fitting basis sets. The reciprocal-space fit for such integrals then indeed becomes problematic due to divergent lattice sums for three-index integrals involving s-GTO fitting functions. However, the actual lattice summations of (5) do not go to infinity, but are effectively truncated by the locality of the CIS coefficients. In our approach, where the direct space images of the CIS vectors are obtained by the back-Fourier-transform,[20] their locality is enforced by restricting the lattice vector $\mathbf{R}_{\mathcal{A}}$ to the Wigner-Seitz supercell (cf. Sec. III). Since no long-range lattice summations are required, the local density-fitting scheme in direct space is more appropriate for the exchange term.

In Paper I, a local-density fitting approach with a single, common, and sufficiently large fit-domain D was employed,

$$({}^{\mathrm{exch}}\mathbf{Vc}) = \sum_{j\mathcal{J}b\mathcal{B}} \sum_{P\mathcal{P}\in D} d^{ij\mathcal{J}}_{P\mathcal{P}}(P\mathcal{P}|a\mathcal{A}b\mathcal{B})c^{j\mathcal{J}}_{b\mathcal{B}}, \quad (19)$$

with the DF-coefficients

$$d^{ij\mathcal{J}}_{P\mathcal{P}} = \sum_{Q\mathcal{Q}\in D} (i\ j\mathcal{J}|Q\mathcal{Q})([J^D]^{-1})_{Q\mathcal{Q}\,P\mathcal{P}}. \quad (20)$$

Here, $J^D_{Q\mathcal{Q}\,P\mathcal{P}}$ is defined as the two-index Coulomb metric matrix within the fit-domain D, i.e., $(P\mathcal{P}|Q\mathcal{Q})\big|_{(P\mathcal{P},Q\mathcal{Q})\in D}$. Such an approach has certain advantages: (i) robust fitting[47,48] is achieved with just the one- rather than the three-term formula (two of the terms in the latter cancel); (ii) only one inversion of the metric matrix in Eq. (20) needs to be computed, and (iii) its implementation, even when exploiting translational symmetry, is not too complicated. On the other hand, the common fit-domain D must be large enough to support all possible $ij\mathcal{J}$- or $a\mathcal{A}b\mathcal{B}$ orbital product distributions in the ERIs of Eq. (5). Consequently, D needs to be somewhat larger (due to $\mathcal{B}$) than the whole Wigner-Seitz supercell, to which the index $\mathcal{A}$ is restricted (*vide infra*). For the 1D polymers this is not problematic, but for 2D slabs, and especially 3D crystals, D would become prohibitively large.

To solve this problem, we have implemented a robust three-term local density fitting scheme with product-density-specific fit-domains, i.e.,

$$\begin{aligned}({}^{\mathrm{exch}}\mathbf{Vc})^{a\mathcal{A}}_i = &\sum_{j\mathcal{J}b\mathcal{B}} \sum_{P\mathcal{P}\in[ij\mathcal{J}]} d^{ij\mathcal{J}}_{P\mathcal{P}}(P\mathcal{P}|a\mathcal{A}b\mathcal{B})c^{j\mathcal{J}}_{b\mathcal{B}} \\ &+ \sum_{j\mathcal{J}b\mathcal{B}} \sum_{P\mathcal{P}\in[a\mathcal{A}b\mathcal{B}]} (ij\mathcal{J}|P\mathcal{P})d^{a\mathcal{A}b\mathcal{B}}_{P\mathcal{P}}c^{j\mathcal{J}}_{b\mathcal{B}} \\ &- \sum_{j\mathcal{J}b\mathcal{B}} \sum_{P\mathcal{P}\in[ij\mathcal{J}]} \sum_{Q\mathcal{Q}\in[a\mathcal{A}b\mathcal{B}]} d^{ij\mathcal{J}}_{P\mathcal{P}}(P\mathcal{P}|Q\mathcal{Q})d^{a\mathcal{A}b\mathcal{B}}_{Q\mathcal{Q}}c^{j\mathcal{J}}_{b\mathcal{B}},\end{aligned} \quad (21)$$

with the two-internal DF coefficients

$$d^{ij\mathcal{J}}_{P\mathcal{P}} = \sum_{Q\mathcal{Q}\in[ij\mathcal{J}]} (i\ j\mathcal{J}|Q\mathcal{Q})([J^{[ij\mathcal{J}]}]^{-1})_{Q\mathcal{Q}\,P\mathcal{P}} \quad (22)$$

and the two-external DF coefficients

$$d^{a\mathcal{A}b\mathcal{B}}_{P\mathcal{P}} = \sum_{Q\mathcal{Q}\in[a\mathcal{A}b\mathcal{B}]} (a\mathcal{A}\,b\mathcal{B}|Q\mathcal{Q})([J^{[a\mathcal{A}b\mathcal{B}]}]^{-1})_{Q\mathcal{Q}\,P\mathcal{P}}. \quad (23)$$

In Eqs. (21)–(23), the summations over auxiliary functions and the dimensions of the metric matrices are restricted to $ij\mathcal{J}$- or $a\mathcal{A}b\mathcal{B}$-density specific fit-domains, denoted as $[ij\mathcal{J}]$, or $[a\mathcal{A}b\mathcal{B}]$, respectively. The (multiple) metric matrices to be inverted (for each $ij\mathcal{J}$- and $a\mathcal{A}b\mathcal{B}$-density) thus are quite small. As demonstrated below in Sec. IV high accuracy in the fit is already achieved with just a few atoms per fit domain.

By exploiting the translational symmetry the above expressions simplify. For example, the expression for the two-external DF coefficients (23) can be rewritten as

$$d^{ab\mathcal{B}''}_{P\mathcal{P}''} = \sum_{Q\mathcal{Q}''\in[ab\mathcal{B}'']} (a\ b\mathcal{B}''|Q\mathcal{Q}'')([J^{[ab\mathcal{B}'']}]^{-1})_{Q\mathcal{Q}''\,P\mathcal{P}''}, \quad (24)$$

with $\mathcal{B}'' = \mathcal{B}\ominus\mathcal{A}$, $\mathcal{P}'' = \mathcal{P}\ominus\mathcal{A}$, and $\mathcal{Q}'' = \mathcal{Q}\ominus\mathcal{A}$.

The first and the second term of Eq. (21) can be treated similarly. The first term then reads as

$$\begin{aligned}&\sum_{j\mathcal{J}b\mathcal{B}} \sum_{P\mathcal{P}\in[ij\mathcal{J}]} d^{ij\mathcal{J}}_{P\mathcal{P}}(P\mathcal{P}|a\mathcal{A}b\mathcal{B})c^{j\mathcal{J}}_{b\mathcal{B}} \\ &\quad= \sum_{P\mathcal{P}\in[ij\mathcal{J}]} \sum_{j\mathcal{J}} d^{i\,j\mathcal{J}}_{P\mathcal{P}} \sum_{b\mathcal{B}'} c^{j}_{b\mathcal{B}'} \\ &\qquad\times (P(\mathcal{P}\ominus\mathcal{A})|a\ b(\mathcal{B}'\ominus\mathcal{A}\oplus\mathcal{J}))\end{aligned} \quad (25)$$

with $\mathcal{B}' = \mathcal{B}\ominus\mathcal{J}$. The second term can be recast as

$$\begin{aligned}&\sum_{j\mathcal{J}b\mathcal{B}} \sum_{P\mathcal{P}\in[a\mathcal{A}b\mathcal{B}]} (ij\mathcal{J}|P\mathcal{P})d^{a\mathcal{A}b\mathcal{B}}_{P\mathcal{P}}c^{j\mathcal{J}}_{b\mathcal{B}} \\ &\quad= \sum_{P\mathcal{P}''\in[ab\mathcal{B}'']} \sum_{j\mathcal{J}} (ij\mathcal{J}|P(\mathcal{P}''\oplus\mathcal{A})) \\ &\qquad\times \sum_{b\mathcal{B}''} d^{ab\mathcal{B}''}_{P\mathcal{P}''}\, c^{j}_{b(\mathcal{B}''\oplus\mathcal{A}\ominus\mathcal{J})}.\end{aligned} \quad (26)$$

Finally, the third term of Eq. (21) can be rewritten as

$$\sum_{j\mathcal{J}b\mathcal{B}} \sum_{P\mathcal{P}\in[ij\mathcal{J}]} \sum_{Q\mathcal{Q}\in[a\mathcal{A}b\mathcal{B}]} d^{ij\mathcal{J}}_{P\mathcal{P}}(P\mathcal{P}|Q\mathcal{Q})d^{a\mathcal{A}b\mathcal{B}}_{Q\mathcal{Q}}c^{j\mathcal{J}}_{b\mathcal{B}}$$
$$= \sum_{j\mathcal{J}} \sum_{P\mathcal{P}\in[ij\mathcal{J}]} d^{i\ j\mathcal{J}}_{P\mathcal{P}} \sum_{b\mathcal{B}''} c^{j}_{b(\mathcal{B}''\oplus\mathcal{A}\ominus\mathcal{J})}$$
$$\times \sum_{Q\mathcal{Q}''\in[ab\mathcal{B}'']} (P(\mathcal{P}\ominus\mathcal{A})|Q\mathcal{Q}'')d^{ab\mathcal{B}''}_{Q\mathcal{Q}''}. \quad (27)$$

The contraction of the two-index integrals $(P(\mathcal{P}\ominus\mathcal{A})|Q\mathcal{Q}'')$ with the two-external DF coefficients $d^{ab\mathcal{B}''}_{Q\mathcal{Q}''}$ in Eq. (27) leads to an object which has exactly the same structure as the two-external integrals $(P(\mathcal{P}\ominus\mathcal{A})|a\ b(\mathcal{B}'\ominus\mathcal{A}\oplus\mathcal{J}))$ of the first term, Eq. (25) (note that $\mathcal{B}'\ominus\mathcal{A}\oplus\mathcal{J}=\mathcal{B}''$). Since the remaining contractions are identical for the first and the third term, this object can simply be added to the two-external integrals of the first term, calculating first and third term contributions to $({}^{\text{exch}}\mathbf{Vc})^{a\mathcal{A}}_i$ in one sweep.

Similar to the Coulomb term, the four-index integrals of Eq. (5) are never assembled (this would nominally scale as $\mathcal{O}(\mathcal{N}^5)$). Instead, the CIS coefficients are first contracted with the two-external three-index integrals [first term, Eq. (25)] or DF coefficients [second term, Eq. (26)]. The results of these contractions are directly assembled to the **Vc** matrix-vector products. Both procedures have a nominal scaling of $\mathcal{O}(\mathcal{N}^4)$.

Evidently, only translationally irreducible sets of three- or two-index objects (i.e., those with the first index belonging to the reference cell) are to be evaluated and explicitly kept. However, these objects are to be correctly translated in the contractions, which leads to a somewhat complicated bookkeeping. Furthermore, note that the calculation of the fitting coefficients Eq. (24) does not involve any translations by $\mathbf{R}_\mathcal{A}$. On the other hand, for the assembly of the matrix-vector product $({}^{\text{exch}}\mathbf{Vc})^{a\mathcal{A}}_i$ such translation vectors do occur in the two-external, and two-internal integrals of Eqs. (25) and (26), respectively. This implies that these integral distributions, primarily the two-external one, are rather large, since $\mathbf{R}_\mathcal{A}$ runs over the whole Wigner-Seitz supercell (*vide infra*).

III. IMPLEMENTATION REMARKS

First of all, we note that in the direct space part of the calculations the translational symmetry is fully exploited (point group symmetry is not yet utilized). This implies that only translationally irreducible direct-space objects, where the first index is restricted to the zero cell, are computed, stored, or read from disk. In contractions involving objects with the first index outside the zero cell, their translationally equivalent counterparts are found and processed instead.

As discussed in Sec. II C, the three-term density fitting scheme used for calculating the exchange term, employs local fit-domains $[ij\mathcal{J}]$ and $[ab\mathcal{B}'']$, specific for each product-density $\rho_{ij\mathcal{J}}$ and $\rho_{ab\mathcal{B}''}$. The fit-domains represent a set of fitting functions, centered on several atoms, such that they provide sufficient support for the densities to be fitted. The fit domains are constructed by using a similar technique as proposed in Ref. 35: for a WF-pair $\phi_i\phi_{j\mathcal{J}}$, or a pair of PAO-atoms $AB\mathcal{B}''$ a quasi-population $q^{ij\mathcal{J}}_{D\mathcal{D}}$, or $q^{AB\mathcal{B}''}_{D\mathcal{D}}$ of the associated product densities on an atom $D\mathcal{D}$ is defined as

$$q^{ij\mathcal{J}}_{D\mathcal{D}} = \sum_{\mu\mathcal{M}\in D\mathcal{D}} [1+P(i,j\mathcal{J})]\left(C_{\mu\mathcal{M}i}\sum_{\nu\mathcal{N}\in D\mathcal{D}} S_{\mu\mathcal{M}\nu\mathcal{N}}C_{\nu\mathcal{N}j\mathcal{J}}\right)^2 \quad (28)$$

or

$$q^{AB\mathcal{B}''}_{D\mathcal{D}} = \sum_{a\in A}\sum_{b\in B\mathcal{B}''}\sum_{\mu\mathcal{M}\in D\mathcal{D}} [1+P(a,b\mathcal{B}'')]$$
$$\times\left(C_{\mu\mathcal{M},a}\sum_{\nu\mathcal{N}\in D\mathcal{D}} S_{\mu\mathcal{M}\nu\mathcal{N}}C_{\nu\mathcal{N},b\mathcal{B}''}\right)^2, \quad (29)$$

respectively. Here, $C_{\nu\mathcal{N},j\mathcal{J}}$ and $C_{\nu\mathcal{N},b\mathcal{B}''}$ are the LCAO coefficients of the WF $j\mathcal{J}$ and PAO $b\mathcal{B}''$, respectively, **S** is the AO overlap matrix, and P is an index permutation operator. Each fit-domain comprises a predefined number N_D of atoms $D\mathcal{D}$ with the highest populations $q_{D\mathcal{D}}$. For all PAO pairs $ab\mathcal{B}''$ belonging to a common pair of atoms $AB\mathcal{B}''$, the same fit-domains $[AB\mathcal{B}'']$ are used. As is shown in Sec. IV, the resulting fit domains are very compact; already with a very low number of atoms N_D per fit domain a very accurate fit is achieved.

The ERIs $(ij\mathcal{J}|P(\mathcal{P}''\oplus\mathcal{A}))$, and $(ab\mathcal{B}''|P(\mathcal{P}\ominus\mathcal{A}))$ in Eqs. (25) and (26) become very small for large $R_\mathcal{J}$, and $R_{\mathcal{B}''}$, respectively, due to the spatial locality of the WFs and PAOs in the respective orbital product densities. The ranges of the cell indices $\mathcal{J}$ and $\mathcal{B}''$ hence can effectively be prescreened on the basis of the quasi-populations defined in Eqs. (28) and (29). In our implementation, the ERIs are evaluated and transformed only for those $\mathcal{J}$ and $\mathcal{B}''$-cells, for which

$$\max_{(D\mathcal{D}\,ij)} q^{ij\mathcal{J}}_{D\mathcal{D}} > T^\mathcal{J}, \text{ and } \max_{(D\mathcal{D}\,AB)} q^{AB\mathcal{B}''}_{D\mathcal{D}} > T^{\mathcal{B}''}, \quad (30)$$

where $T^\mathcal{J}$ and $T^{\mathcal{B}''}$ are appropriate thresholds. It turns out that the convergence of the resulting excitation energies with respect to $T^{\mathcal{B}''}$ is relatively slow, despite reasonably good localization of the PAOs. Therefore, in order to reach meV convergence in the CIS excitation energies several spheres of lattice vectors $\mathcal{B}''$ need to be included.

The ranges of the fitting functions $P\mathcal{P}$ and $P\mathcal{P}''$ in the fitting coefficients $d^{ij\mathcal{J}}_{P\mathcal{P}}$ and $d^{ab\mathcal{B}''}_{P\mathcal{P}''}$ are restricted to the corresponding fit-domains, i.e., $P\mathcal{P}\in[ij\mathcal{J}]$ and $P\mathcal{P}''\in[ab\mathcal{B}'']$, and thus are relatively small and close to the zeroth unit cell. In particular, the dependence on $R_\mathcal{A}$ drops out, on going from Eq. (23) to Eq. (24). This, however, is not the case for the three-index ERIs, which are contracted with these coefficients in Eqs. (25) and (26). Here, the dependence on $\mathbf{R}_\mathcal{A}$ remains, and the ranges of the fitting functions are substantially extended due to addition of all possible $\mathbf{R}_\mathcal{A}$ vectors. These $\mathbf{R}_\mathcal{A}$ appear in the final matrix-vector product $(\mathbf{Hc})^{a\mathcal{A}}_i$, and thus in the residual vector; the $\mathcal{A}$ range hence reflects the locality of the exciton.

The $\mathcal{B}''$ and $\mathcal{A}$ ranges thus are the two critical parameters influencing the size of the $(ab\mathcal{B}''|P(\mathcal{P}\ominus\mathcal{A}))$ integral distribution. Calculation (transformation), storage, and reading of these ERIs presently constitutes the computational bottleneck in terms of central processing unit (CPU) time, input/output,

memory, and disk resources. The transformation of the three-index ERIs from AO to PAO basis is done similarly as for the $(ia\mathcal{A}|P\mathcal{P})$ ERIs used for local second-order Møller-Plesset perturbation theory (LMP2).[31] However, since there are substantially more PAOs per cell than WFs, and since the former are usually less localized, the number of half-transformed ERIs is much larger in the present, than in the LMP2 case. Therefore, an efficient transformation procedure requires a lot of memory, and, in addition, special paging techniques.

As is explained in Sec. II A, the range for the $\mathcal{A}$-cells is restricted to the WS supercell. Moreover, each WF ϕ_i possesses its own WS supercell, hence, its own $\mathcal{A}$ range. Since the ERIs $(ab\mathcal{B}''|P(\mathcal{P}\ominus\mathcal{A}))$ appearing in Eq. (25) do not explicitly refer to index i, the index $\mathcal{A}$ here is element of the union of all WS supercells belonging to different i. Yet, because all i are restricted to the zero cell the union of all WS supercells belonging to different i is not much larger than the individual Wigner-Seitz supercells themselves. The implications on the size of this integral set thus are not excessive.

IV. CALCULATIONS AND DISCUSSION

The method as described above has been applied to several 3D test systems ranging from wide-gap insulators to semiconductors. These comprise crystals with different types of bonding, i.e., hydrogen bonded orthorhombic ice, the ionic crystals LiH, MgO, and LiF, and the covalent crystals diamond, SiC, and Si. Double zeta quality basis sets are utilized in this work, which are derived from the corresponding molecular cc-pVDZ basis sets[49,50] or taken from some previous periodic studies.[51,52] Detailed structural and basis set descriptions are provided as supplementary material.[53]

A. Convergence with respect to the parameters of the computational scheme

Density fitting with a common, sufficiently large fit-domain, used for all orbital product densities to be fitted, has been employed in Paper I for the 1D case. There, it was shown that a sufficiently high accuracy of the fitting was achieved already with a small fitting basis set, e.g., a GTO cc-pVDZ DF-MP2 fitting basis[54] converted into the mixed cc-pVDZ GTO/PTO basis[35] for a DZ+P AO basis set. The same holds true also for the 3D case based on our local fitting scheme with much smaller, density-specific fit domains and the robust three-term formula (*vide supra*): e.g., for a CIS calculation on the LiF crystal in a DZ+P AO basis, extending the fitting basis set from VDZ to VTZ quality affects the excitation energies only in the sub-microhartree range. As is evident from Table I, the resulting excitation energies are very insensitive with respect to the fit-domain size (already a very few atoms in the fit domain suffice for microhartree-accuracy). A default threshold of 6 atoms appears as a very conservative choice, and has been employed in all further calculations. Additional atoms are added to these domains for particular densities, if dictated by their symmetry. Interestingly, for the density-fitted periodic LMP2 method, based on local density fitting, microhartree accuracy in the correlation energy is only achieved when using somewhat larger fit-domains.[35]

TABLE I. Singlet and triplet CIS excitation energies depending on the fit domain size. The given domain sizes are the minimal domain sizes plus symmetry related atoms. The energies for LiF and MgO are calculated with a $5\times5\times5$ and $6\times6\times6$ cells in the WS supercell, respectively, and a threshold $T^{\mathcal{B}''}=10^{-5}$.

	ω_S (eV)		ω_T (eV)	
Domain size	MgO	LiF	MgO	LiF
2	11.9208	15.8371	11.2565	15.1146
4	11.9209	15.8371	11.2566	15.1144
6	11.9209	15.8371	11.2567	15.1143
8	11.9209	15.8370	11.2567	15.1142
12	11.9210	15.8371	11.2567	15.1142

Other important parameters of the current scheme are the thresholds $T^{\mathcal{J}}$ and $T^{\mathcal{B}''}$ defining the ranges for the three-index integrals to be evaluated and processed according to the spatial proximity of WF ϕ_i to WF $\phi_{j\mathcal{J}}$ or PAO ϕ_a to PAO $\phi_{b\mathcal{B}}$, respectively (see Sec. III). The two-internal ERIs $(ij\mathcal{J}|P(\mathcal{P}''\oplus\mathcal{A}))$ are relatively inexpensive and not numerous, and therefore can be calculated with tight $T^{\mathcal{J}}$ without too much effort. Moreover, the results turned out to be insensitive with respect to this threshold. In all reported calculations, a value of $T^{\mathcal{J}}=10^{-5}$ was used.

Yet for the two external ERIs $(ab\mathcal{B}''|P(\mathcal{P}\ominus\mathcal{A}))$ the situation is different: tightening the $T^{\mathcal{B}''}$-threshold noticeably increases the size of this integral distribution, making the calculation considerably more expensive. Unfortunately, as shown in Table II, the convergence of the excitation energies with respect to this threshold is relatively slow: with $T^{\mathcal{B}''}=10^{-4}$ the error can still be as large as 0.1 eV. A similar behaviour was observed also for other test systems (SiC, Si, LiH). Thus, a rather conservative value of $T^{\mathcal{B}''}=10^{-5}$ has been employed in the subsequent calculations. Compared to $T^{\mathcal{B}''}=10^{-4}$ this implies on average an increase in the computing time by about 40%, but the error reduces to a few hundredths of an eV.

B. Localization of the CIS coefficients

The physical nature of an exciton manifests itself (i) in the localization of the CIS coefficients in the reciprocal-space canonical representation with respect to the band and

TABLE II. Singlet and triplet CIS excitation energies of MgO and LiF (calculated with $6\times6\times6$ and $5\times5\times5$ cells in the WS supercell, respectively) for different values of the threshold $T^{\mathcal{B}''}$.

	ω_S (eV)		ω_T (eV)	
$T^{\mathcal{B}''}$	MgO	LiF	MgO	LiF
10^{-2}	12.3243	15.9471	11.6740	15.2305
10^{-3}	12.1917	15.9249	11.5163	15.1960
10^{-4}	11.9785	15.8476	11.3068	15.1229
10^{-5}	11.9209	15.8371	11.2567	15.1143
10^{-6}	11.8781	15.8345	11.2176	15.1117
10^{-7}	11.8687	15.8344	11.2101	15.1117

k-vector indices, and (ii) in their spatial localization in the direct-space representation. These characteristics influence various physical properties, as well as the computational effort needed to correctly evaluate the corresponding excitation energies.

1. Localization in reciprocal space

The relative contributions of the squared CIS coefficients related to different bands (summed over the **k**-points), of the CIS wavefunctions calculated for the SiC and MgO crystals, are shown in Fig. 1. Since the lowest excited states in these systems are degenerate (triply degenerate in MgO, and doubly in SiC) the contributions are averaged over these states. It is seen that for the lowest excited states the major contribution comes from the LUCO-band, while the other unoccupied bands virtually do not contribute. Indeed, exclusion of all the virtual bands apart from the LUCO-band affects the CIS excitation energy only marginally, i.e., it increases by only 0.5 eV in MgO, and by 0.6 eV in SiC.

A modification of the AO basis set itself, on the other hand, has a much larger impact on the resulting energies: as was shown in Ref. 55 for the case of the MgO crystal, a variation of the exponent of only one *sp*-shell of the AOs centered on the Mg atoms reduces the excitation energy by nearly 2 eV. This originates from the fact that the standard basis sets, optimized for the ground state, are suboptimal for excited states, which leads to an unbalanced description of ground and excited states, and thus to a substantial overestimation of the excitation energies. In molecular calculations, this problem is usually alleviated by augmenting the basis set with diffuse functions, which in many cases returns the desired balance, although Rydberg states are often overcorrected.

For solids, due to linear dependencies, diffuse orbitals are difficult to process, and, furthermore, hardly useful in 3D-packed systems.[55,56] This is quite a general issue for AO-based calculations of excited states, asking, in our view, for considerable attention in the future.

The limited size of the virtual space required for a proper description of the lowest CIS state, as illustrated in Fig. 1, unfortunately cannot straightforwardly be exploited in our scheme, since a truncation of the virtual space in reciprocal space to specific bands does not translate to a corresponding truncation of the PAOs in direct space. Possibly, the virtual space could be represented by a limited number of specially constructed Wannier functions, designed to reproduce the low-lying virtual bands as accurately as possible,[57–59] yet this was not tried in the present work. The CIS method presented here is meant as an integral part of a higher-order correlated treatment, which in turn will demand a rich virtual space to properly describe electron correlation effects.

The canonical CIS coefficients, as displayed in Fig. 2, are also localized with respect to the **k**-vectors within the respective band, yet not as pronounced as with respect to the band index. The CIS coefficients of the lowest energy excitons of MgO tend to localize around the Γ-point, while those of SiC around the X-point of the BZ, which in both cases correlates with the position of HOCO-LUCO energy difference minimum.

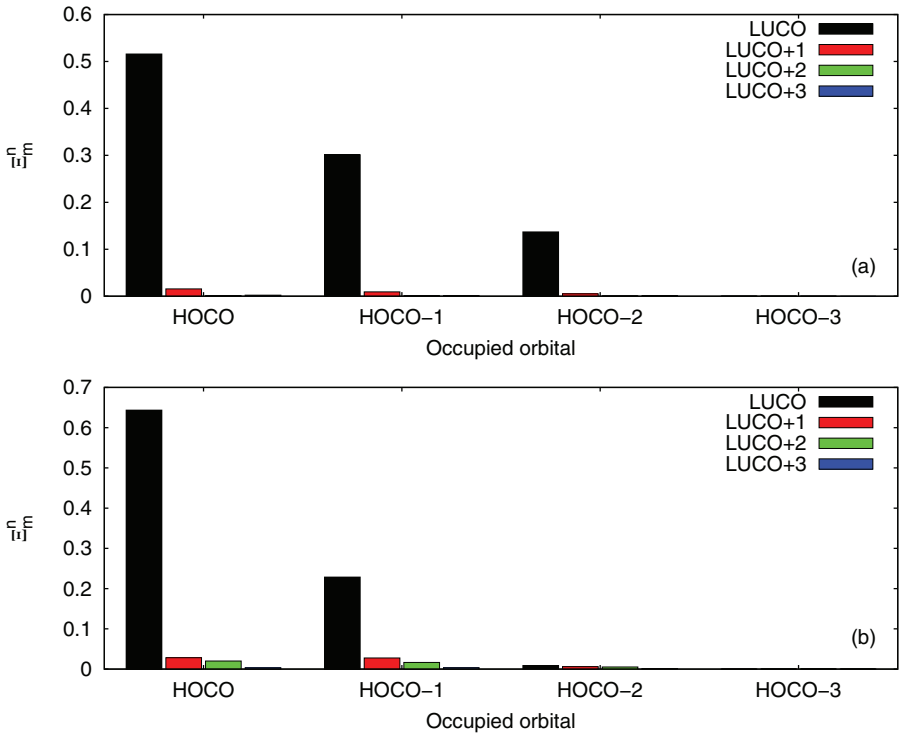

FIG. 1. The CIS coefficients in canonical space. The columns show a HOCO-band−n to a LUCO-band+m ($m, n = 0, 1, 2, 3$) contribution to the squares of the CIS coefficient of the singlet state (summed over all **k**-points) $\Xi_m^n = \sum_{\mathbf{k}} |c_{\mathrm{LUCO}+m}^{\mathrm{HOCO}-n}(\mathbf{k})|^2$. The contributions are averaged over the 3 and 2 degenerate excitonic states in (a) MgO and (b) SiC, respectively.

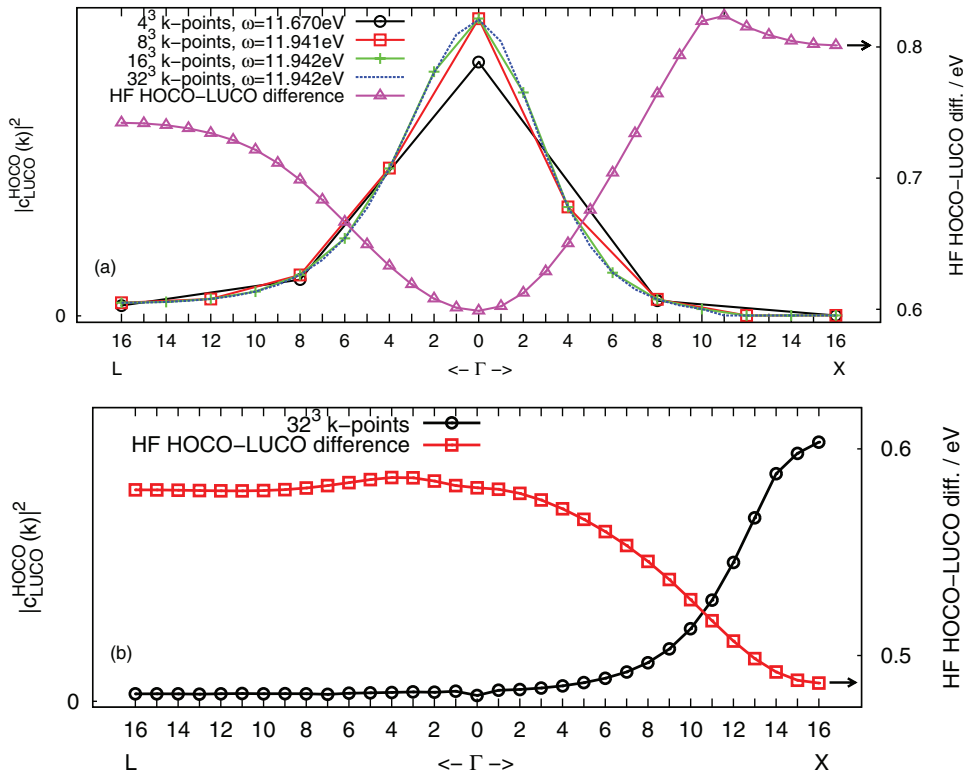

FIG. 2. HOCO-LUCO contribution to the CIS wavefunction, $|c^{\mathrm{HOCO}}_{\mathrm{LUCO}}(\mathbf{k})|^2$, of (a) MgO and (b) SiC and corresponding HF HOCO-LUCO differences. In the case of MgO different **k**-meshes are taken.

The degeneracy of the HOCO of MgO at the Γ-point is 3, while the related LUCO is not degenerate. Therefore, the orbital energies of the HOCO, HOCO-1, and HOCO-2 bands around the Γ-point are quite close, implying that the weights of the determinants related to these orbitals are similar. This explains why in Fig. 1 the excitations from the three uppermost occupied bands of MgO have similar weight in the CIS wavefunction. The bands HOCO-3 and LUCO+1, on the other hand, are energetically well separated from HOCO and LUCO, respectively, within this region of the BZ. Hence, the weights of the determinants related to these bands are much smaller compared to the weights related to excitations from HOCO, HOCO-1, or HOCO-2 to LUCO.

A similar situation occurs for the SiC crystal, with the sole difference that the essential contributions come from **k**-vectors in the vicinity of the X-point. The HOCO state is doubly degenerate there, while the LUCO state is again non-degenerate. Therefore, only excitations from HOCO and HOCO-1 to LUCO are mainly involved in building the CIS wavefunction related to the lowest state.

The better the localization of the CIS coefficients in the **k**-space is, i.e., the less smooth these coefficients as a function of **k** are, the denser a uniform **k**-grid has to be chosen for the numerical quadrature over the BZ (cf. Sec. III for a detailed discussion). The degree of localization of the CIS coefficients in the **k**-space (non-smoothness as a function of **k**) relates conversely to their localization in direct space, which in turn is related to the electron-hole attraction. It thus provides a measure for the nature of the exciton. Moreover, the localization of the CIS coefficients in direct space determines to large extent the computational resources needed to perform the calculation. Indeed, in order to obtain a converged value for the excitation energy the Wigner-Seitz supercell truncating the $\mathbf{R}_{\mathcal{A}}$ vectors must be chosen large enough that it covers all non-negligible CIS coefficients $c^i_{a\mathcal{A}}$, making delocalized excitons more difficult to treat.

2. Localization in direct space

Figure 3 displays a histogram of the maximal CIS coefficients $\max_{ia}|c^i_{a\mathcal{A}}|$ for different distances between a WF and a PAO. Evidently, the localization of the exciton correlates with the value for the bandgap (cf. Sec. IV D). Among the systems considered here, the most localized exciton is observed for the wide-gap insulator LiF, while the localization of the exciton in the semiconductor Si is the weakest. Interestingly, despite a lesser localization of the exciton in Si relative to that in diamond in terms of the absolute distance; both excitons have very similar localization in terms of the number of unit cells to be included in the Wigner-Seitz supercell. The computational cost hence is similar for both systems. For all exemplary systems ranging from wide-gap insulators to semiconductors, the lowest-energy excitons are all reasonably well localized, such that they can be treated with the proposed approach.

3. Reciprocal space vs. direct space localization

In Subsections IV B 1 and IV B 2, it was shown that the character of the (lowest) excited CIS states implies both localization in direct (position vector) and reciprocal (energy) spaces. Here, we discuss the origins of this localization.

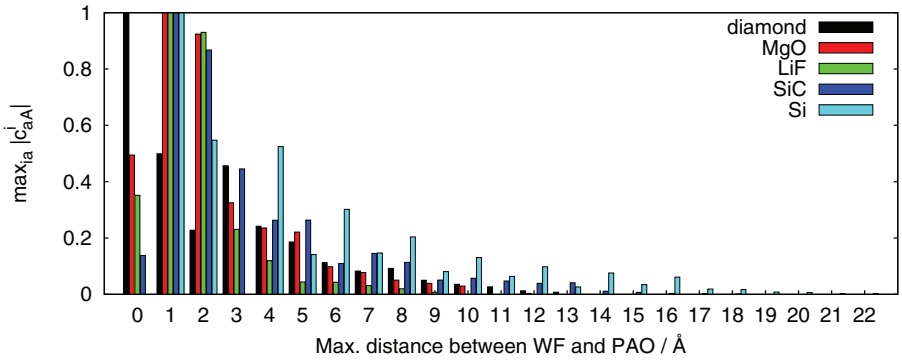

FIG. 3. The maximal CIS coefficients in direct space against the maximal distance between WF and PAO, $\max_{ia}|c^i_{a,A}|$, for the singlet states of diamond, MgO, LiF, SiC, and Si.

In atoms or small molecules, excited states possess either Rydberg or local character. In the former case, the excited electron is very delocalized and moves in a field of a point-like positive ion, while in the latter case the excited state density is more or less localized around the atom or the small molecule. The CIS description includes the zeroth-order orbital energy differences, the first-order interaction between the electron-hole dipoles (the Coulomb term, which is usually destabilizing, but small), and the attractive interaction between the excited electron and its hole (the exchange term). For locally excited states on the one hand, the electron-hole attraction is sizable since the excited electron is spatially close to the hole. On the other hand, for Rydberg states the excited electron is farther away from the hole, and the attractive excitonic attraction is much lower. At the same time, Rydberg states, which predominantly involve diffuse virtuals, benefit from lower orbital energy differences in the zeroth-order term.

Inclusion of electron correlation on top of CIS obviously corrects the description of the excited state. However, the effects of screening of the excited electron from its hole by other electrons (which is a correlation effect) is not strong in neither of these two cases, particularly not for Rydberg states. Nevertheless, usually the overall correlation effects in the excited state exceed those in the ground state, and consequently, the uncorrelated CIS treatment then overestimates the excitation energy. Yet in certain cases the excited state correlation energy happens to be of a similar or even smaller magnitude than that of the ground state. In such cases, the CIS method benefits from an effective error compensation and either delivers quite accurate excitation energies (cf., e.g., the low-lying Rydberg states of ethylene[60]), or even underestimates the excitation energy (cf., e.g., the lowest triplet state of ethylene[60]).

Let us now consider a crystal formed from atoms or small molecules. Rydberg states obviously do not occur in such an infinite bulk structure. Bloch waves of locally excited states of the individual molecules, on the other hand, do exist in the crystal. For such a local state the electron-hole attraction is expected to remain rather large, i.e., of about the magnitude as in the isolated molecule. However, the zeroth-order orbital energy difference contribution in a crystal requires some consideration: when individual molecules condense to a periodic structure the molecular energy levels transform into bands, whose widths depend on the strength of the interaction between the individual molecules. Localization of an exciton in direct space necessitates delocalization in the reciprocal space, implying that not minimal orbital energy differences throughout the highest valence and lowest conduction bands constitute a fairly large destabilizing contribution to the excitation energy. In other words, a large attractive excitonic effect implies a large destabilizing zeroth-order contribution and, vice versa, a minimal zeroth-order contribution the complete loss of any attractive excitonic effect. Consequently, the variational principle tries to find an optimal compromise between the two counteracting contributions. In doing so, the localization in the direct space is partially sacrificed in order to concentrate the exciton in the reciprocal space around **k**-points with minimal difference between HOCO and LUCO bands.

This is illustrated by a calculation on the ice crystal, where the converged CIS coefficients of a molecular calculation (for technical reasons we had to use a water tetramer rather than a single water molecule) are used as the starting guess for a periodic CIS calculation on ice (cf. Table III). Evidently, in the zeroth iteration of the periodic CIS calculation the Coulomb and exchange terms (the latter reflecting the attractive excitonic effect) are very similar to the corresponding values in the molecular calculation, whereas the zeroth-order orbital energy difference contribution is much larger (25.2 rather than 20.3 eV). In the course of the iterations of the

TABLE III. The HOCO-LUCO (HOMO-LUMO) energy and CIS lowest singlet excitation energy, partitioned in the orbital-energy-difference (Fock), Coulomb and exchange contributions for (i) a cluster of four water molecules cut from the ice crystal, (ii) the ice crystal with the converged four-molecule cluster CIS solution, and (iii) the ice crystal with the converged periodic CIS solution. The energies are given in eV.

		Solid	
	Four-molecule cluster	Cluster CIS solution	Periodic CIS solution
HOMO-LUMO/HOCO-LUCO	17.51	17.75	
CIS	9.60	14.81	12.18
Fock (**cFc**)	20.30	25.15	21.32
Coulomb ($\mathbf{c}^{\text{coul}}\mathbf{Vc}$)	0.87	0.80	0.52
Exchange ($\mathbf{c}^{\text{exch}}\mathbf{Vc}$)	− 11.57	− 11.14	− 9.66

periodic CIS calculation, the zeroth-order contribution reduces to 21.3 eV, at the price of increasing the excitonic contribution from −11.1 to −9.7 eV. Notably, the lowest CIS state of the molecular calculation (which cannot be a Rydberg state since no diffuse basis functions were included in this calculation) is actually lower than that of ice.

Such a reduced direct space localization of the exciton as it occurs in the crystal is actually reminiscent of intramolecular charge transfer states in large molecules. Since the excited electron is on average localized at a certain distance from its hole, the other electrons effectively screen the electron-hole attraction. Such a screening (which is absent or very small in local or Rydberg states) is a pure correlation effect and not included in the CIS description. It eases delocalization of the exciton, thus lowering the exciton energy for such states. For charge transfer states in large molecules, CIS is known to overestimate the excitation energy, in some cases quite substantially, in agreement with the analysis outlined here. In solids, where screening effects are considerably stronger due to the 3D dimensionality,[61] the overestimation of CIS is expected to be even larger.

C. Convergence with respect to reciprocal space sampling and Wigner-Seitz supercell size

In Sec. II A, two finite models of a crystal, namely, the cyclic model[20,36,37] and WSS-TIM were discussed. Here, we investigate the convergence of the excitation energies with respect to the truncation parameter within both models. Figure 4 displays, for the cases of the MgO and SiC crystals, the calculated excitation energies as a function of the Wigner-Seitz supercell, (i) for the cyclic model, and (ii) for the WSS-TIM with a very dense **k**-mesh (15 × 15 × 15, and 16 × 16 × 16 for SiC and MgO, respectively). Evidently, for the WSS-TIM the convergence of the excitation energies to the infinite crystal values is much better than for the pure cyclic model. Already for a Wigner-Seitz supercell corresponding to **k**-meshes of modest density (7 × 7 × 7 for SiC and 5 × 5 × 5 for MgO) the resulting excitation energies are essentially converged. The error of the cyclic model thus originates mainly from an inadequate quadrature over the BZ. Increasing the density of the **k**-mesh is, as already stated above, computationally inexpensive, but significantly improves the quality of the calculation. At the same time, due to spatial localization of the CIS coefficients $c^i_{a\mathcal{A}}$ in direct space (cf. Fig. 3), restricting them [and their matrix-vector products $(\mathbf{Hc})^{a\mathcal{A}}_i$] to a finite Wigner-Seitz supercell, i.e., truncating $\mathbf{R}_{\mathcal{A}}$, causes a much smaller error.

The importance of the improved BZ quadrature is also illustrated by Fig. 2 showing the locality of the (most important) HOCO-LUCO contribution to the CIS vector in the BZ: apparently only 16^3 **k**-points provide sufficient support to accurately describe it along the L-Γ-X direction.

D. Comparison to experiment

Table IV compares the lowest CIS excitation energies to the corresponding experimental values of our set of test systems. The used threshold of $T^{\mathcal{B}''} = 10^{-5}$ (cf. Secs. III and IV A), as well as the obtained value for the norm of the

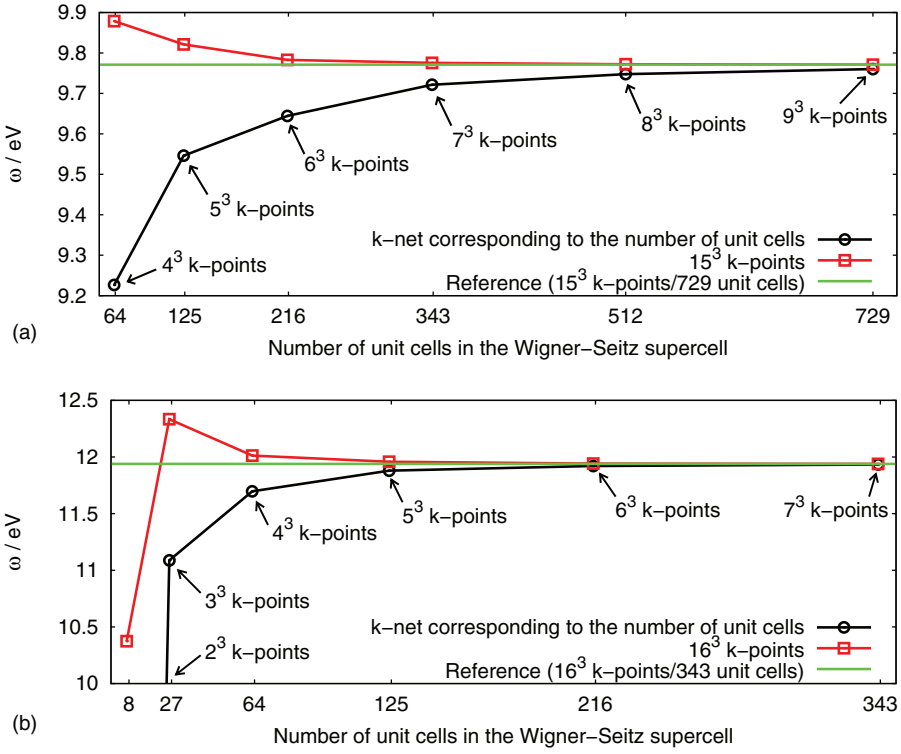

FIG. 4. Singlet state excitation energies of (a) SiC and (b) MgO as a function of the number of unit cells included in the direct space description of the exciton. Calculations are performed for the cyclic model (black curves with dots), and for the WSS-TIM with a very dense **k**-mesh (15 × 15 × 15, and 16 × 16 × 16 for SiC and MgO (red curves with squares), respectively). The reference values are obtained by employing the WSS-TIM, employing a 15 × 15 × 15 **k**-mesh with a Wigner-Seitz supercell of 729 unit cells (SiC), and a 16 × 16 × 16 **k**-mesh with a supercell of 343 unit cells (MgO), respectively (horizontal green lines).

TABLE IV. Experimental direct optical and fundamental bandgaps, vertical Hartree-Fock HOCO-LUCO differences (E_g^{HF}), Γ-point CIS excitation energies for the lowest singlet and triplet states and corresponding norms of the CIS vector in direct space.[20] The energies are given in eV.

				Singlet		Triplet	
System	Exp. (optical)	Exp. (fundamental)	E_g^{HF}	ω	Norm	ω	Norm
LiH	4.9[a],5.0[b]	–	12.82	7.68	0.9993	7.13	0.9997
Ice	8.6[c]	10.9[c]	18.28	12.18	0.9999	11.42	1.0000
Diamond	6.4[d,e], 7.2[e,f]	6.5[d], 7.3[f]	14.65	11.72	0.9916	10.34	0.9981
MgO	7.7[g], 7.6[h]	7.8[g], 8.7[h]	16.29	11.94	0.9993	11.27	0.9997
LiF	12.6[i]	13.6[i], 14.2[j]	22.40	15.84	1.0000	15.12	1.0000
SiC	6.0[e,k], 7.0[e,f]	6.0[k], 7.0[f]	13.80	9.74	0.9957	9.29	0.9967
Si	4.2[d,e], 3.5[e,f]	4.2[d], 3.5[f]	8.43	6.05	0.9886	5.62	0.9917

[a]Reference 64.
[b]Reference 65.
[c]Reference 66.
[d]Reference 67.
[e]Estimated on the basis of the indirect exciton binding energy.
[f]Reference 68.
[g]Reference 69.
[h]Reference 70.
[i]Reference 71.
[j]Reference 72.
[k]Reference 73.

exciton in direct space representation (cf. Paper I) suggest, that the values for the CIS excitation energies are converged up to a few hundredths of an eV with respect to the size of the Wigner-Seitz supercell and the $T^{\mathcal{B}''}$ threshold.

There is a certain scatter in the experimental values reported in the literature (by more than 1 eV). Furthermore, for indirect bandgap systems (in our case C, Si, and SiC), we were not able to find experimental values for the direct optical bandgaps, which correspond to Γ-point excitons. The values of the experimental optical bandgaps given in Table IV for these three systems are obtained by subtracting the indirect exciton binding energies (which are for these crystals in fact very small) from the direct fundamental bandgaps.

In any case, it is evident, that the CIS method grossly overestimates the experimental excitation energies. The largest error of about 5 eV was observed for diamond. This is in accord with the TD-HF results of Ref. 15. In molecular calculations, the errors of the CIS method usually do not exceed 1-2 eV, at least for the lowest valence states without charge-transfer character. There are two possible origins of the larger discrepancy for solids, as observed in our calculations.

First of all, the CIS description lacks dynamical electron correlation effects. As is discussed in Sec. IV B 3, in solids the excited states are relatively delocalized and resemble molecular charge-transfer rather than local or Rydberg states. The CIS error due to the neglect of screening in charge-transfer excited states is usually quite significant in molecules, and in 3D crystals it is expected to be even larger. The main reason is the inadequate zeroth order description of the fundamental bandgap in terms of the uncorrelated Hartree-Fock HOCO-LUCO orbital energy difference. Also the excitonic effect is considerably overestimated by CIS due to the lack of screening, but this helps to some extent to counterbalance the much too large zeroth order contribution. The first order CIS method clearly provides an improvement over the zeroth order orbital energy difference treatment: the CIS excitation energy is substantially closer to the optical bandgap than the HOCO-LUCO difference to the fundamental bandgap. Inclusion of electron correlation (screening) is expected to correct the CIS description of optical bandgaps, and even more so the estimates for electron affinities and ionization potentials (cf., e.g., Ref. 62, which reports MP2-level correlation corrections to the fundamental bandgap exceeding 10 eV for diamond).

The second major problem severely affecting the accuracy of calculated bandgaps in solids is the AO basis set deficiency. In molecular calculations, this problem can usually be circumvented by augmenting the AO basis by diffuse functions. Yet such a strategy is difficult or even impossible in 3D packed systems due to linear dependencies in the augmented basis. The AO basis sets commonly used in periodic calculations are clearly biased towards the electronic ground state, which leads to a further overestimation of the excitation energy. As already mentioned in Sec. IV B, and demonstrated in Ref. 55, tweaking the basis set by lowering the exponent of one AO type significantly affects the position of the lower conduction bands and thus leads to a sizable decrease of the bandgap. We note in passing that an improvement of the basis set not necessarily implies a lower CIS bandgap: as an example, we employed the Ahlrichs valence triple-zeta basis set[63] in a calculation on MgO. Although the HOCO-LUCO difference dropped by around 0.5 eV relative to the value of 16.3 eV of Table IV, the CIS bandgap nevertheless increased by 0.2 eV to 12.2 eV.

Comparison of our AO based HOCO-LUCO differences with those of the plane wave Hartree-Fock calculations reported in Ref. 62 (for Si, SiC, and C the indirect bandgaps, which are in our case 7.65 eV, 9.82 eV, and 12.56 eV, respectively, should be compared) reveals a discrepancy of up to an eV. In most cases, the HOCO-LUCO differences of the plane wave calculations are smaller, which again illustrates the bias of AO basis sets towards the electronic ground state.

Both issues, i.e., the lack of dynamical electron correlation, and the basis set problem, will be addressed in future work.

V. CONCLUSIONS

In this contribution, we presented theory, implementation, and first results for a general 3D periodic density-fitted local CIS method. The method is a generalization of a 1D periodic CIS method presented recently. The Davidson diagonalization of the CIS Hamiltonian matrix is carried out in reciprocal space, while the diagrams of the residual calculation are evaluated partially in the direct, and partially in the reciprocal space. For the Coulomb diagram describing exciton-exciton interaction an Ewald technique was utilized to efficiently carry out the necessary infinite lattice summations. The exchange diagram describing the electron-hole interaction is calculated entirely in direct space, employing a robust product-density specific density fitting scheme. The sparsity due to the spatial locality of the orbitals and CIS coefficients is fully utilized.

All the calculations presented in this paper were performed by using a serial version of our program. The computational time is mainly determined by the size of the Wigner-Seitz supercell, i.e., by the locality of an exciton. The calculations took from a few hours (for the relatively well localized exciton in LiF, where a $6 \times 6 \times 6$ supercell was sufficient) to a few days for Si (where a $9 \times 9 \times 9$ supercell was needed). Note that for larger unit cells smaller Wigner-Seitz supercells can be used to capture an exciton of a certain locality. For example, for ice, already a $3 \times 3 \times 3$ supercell was sufficient. The present bottleneck of the calculations are evaluation, sorting, and storage of the three-index ERIs $(ab\mathcal{B}''|P(\mathcal{P} \ominus \mathcal{A}))$ (cf. Sec. II C and III).

The reciprocal-space parts of the calculation are inexpensive, which allows for the use of dense **k**-meshes, decoupled from the actual size of the WS supercell via the Wigner-Seitz supercell truncated infinite model, WSS-TIM. It turns out that such a decoupling is very beneficial, leading to much quicker convergence of the resulting excitation energies with respect to the size of the underlying supercell in direct space.

The CIS method itself, although substantially improving the zeroth-order bandgap energy (i.e., the HOCO-LUCO energy difference), still noticeably overestimates the experimental bandgaps by several eV. Reasons for this are (i) the lack of dynamical correlation effects (screening), and (ii) deficiencies in the AO basis sets. The CIS method presented here, is to be seen as the first building block of a more elaborate treatment including dynamical correlation effects via, e.g., local CIS(D)[74] or CC2[75–77] methods. A promising possibility to fix the problem of AO basis set deficiencies would be to augment the AO basis sets by a small amount of plain waves (with low energy cutoff). Another route to explore is the combination of the present periodic CIS method with TD-DFT (or its Tamm-Dancoff approximation) in the framework of a long-range–short-range separation of the electron-electron interaction operator.[78]

ACKNOWLEDGMENTS

The authors thank Matteo Ferrabone, Cesare Pisani, and Roberto Dovesi for useful discussions. Financial support from the Deutsche Forschungsgemeinschaft (DFG), in the context of the priority program 1145, is gratefully acknowledged.

[1] S. Hirata, M. Head-Gordon, and R. J. Bartlett, J. Chem. Phys. **111**, 10774 (1999).
[2] A. F. Izmaylov and G. E. Scuseria, J. Chem. Phys. **129**, 034101 (2008).
[3] L. Hedin, Phys. Rev. **139**, A796–A823 (1965).
[4] G. Onida, L. Reining, and A. Rubio, Rev. Mod. Phys. **74**, 601–659 (2002).
[5] M. Rohlfing and S. G. Louie, Phys. Rev. Lett. **81**, 2312–2315 (1998).
[6] P. H. Hahn, W. G. Schmidt, M. Preuss, K. Seino, F. Bechstedt, and J. Bernholc, Phys. Rev. Lett. **94**, 037404 (1994).
[7] M. Shishkin, M. Marsman, and G. Kresse, Phys. Rev. Lett. **99**, 246403 (2007).
[8] K. Hummer, P. Puschnig, and C. Ambrosch-Draxl, Phys. Rev. Lett. **92**, 147402 (2004).
[9] F. Sottile, M. Marsili, V. Olevano, and L. Reining, Phys. Rev. B **76**, 161103 (2007).
[10] M. Palummo, O. Pulci, R. Del Sole, A. Marini, P. Hahn, W. G. Schmidt, and F. Bechstedt, J. Phys.: Condens. Matter **16**, S4313 (2004).
[11] S. Hirata and R. J. Bartlett, J. Chem. Phys. **112**, 7339 (1999).
[12] H. Katagiri, J. Chem. Phys. **122**, 224901 (2005).
[13] I. Gadaczek, K. J. Hintze, and T. Bredow, Phys. Chem. Chem. Phys. **14**, 741–750 (2012).
[14] C. Buth, U. Birkenheuer, M. Albrecht, and P. Fulde, Phys. Rev. B **72**, 195107 (2005).
[15] L. Bernasconi, S. Tomić, M. Ferrero, M. Rérat, R. Orlando, R. Dovesi, and N. M. Harrison, Phys. Rev. B **83**, 195325 (2011).
[16] H. Stoll, Phys. Rev. B **46**, 6700–6704 (1992).
[17] V. Bezugly and U. Birkenheuer, Chem. Phys. Lett. **399**, 57–61 (2004).
[18] P. Fulde, Theor. Chem. Acc. **114**, 255–258 (2005).
[19] A. Stoyanova, L. Hozoi, P. Fulde, and H. Stoll, J. Chem. Phys. **131**, 044119 (2009).
[20] M. Lorenz, D. Usvyat, and M. Schütz, J. Chem. Phys. **134**, 094101 (2011).
[21] V. R. Saunders, C. Freyria-Fava, R. Dovesi, L. Salasco, and C. Roetti, Mol. Phys. **77**, 629 (1992).
[22] C. M. Zicovich-Wilson, R. Dovesi, and V. R. Saunders, J. Chem. Phys. **115**, 9708 (2001).
[23] S. Casassa, C. M. Zicovich-Wilson, and C. Pisani, Theor. Chem. Acc. **116**, 726–733 (2006).
[24] S. Sæbø and P. Pulay, Chem. Phys. Lett. **113**, 13–18 (1985).
[25] M. Schütz, G. Hetzer, and H.-J. Werner, J. Chem. Phys. **111**, 5691 (1999).
[26] D. Usvyat, L. Maschio, C. Pisani, and M. Schütz, Z. Phys. Chem. **224**, 441–454 (2010).
[27] E. R. Davidson, J. Comput. Phys. **17**, 87–94 (1975).
[28] S. B. Trickey, J. A. Alford, and J. C. Boettger, *Computational Materials Science, Theoretical and Computational Chemistry series* (Elsevier, Oxford, 2004), Vol. 15.
[29] S. Varga, Phys. Rev. B **71**, 073103 (2005).
[30] M. Milko, J. Noga, and S. Varga, Int. J. Quantum Chem. **107**, 2158–2168 (2007).
[31] L. Maschio, D. Usvyat, F. R. Manby, S. Casassa, C. Pisani, and M. Schütz, Phys. Rev. B **76**, 075101 (2007).
[32] C. Pisani, L. Maschio, S. Casassa, M. Halo, M. Schütz, and D. Usvyat, J. Comput. Chem. **29**, 2113–2124 (2008).
[33] S. Varga, Int. J. Quantum Chem. **108**, 1518–1527 (2008).
[34] A. M. Burow, M. Sierka, and F. Mohamed, J. Chem. Phys. **131**, 214101 (2009).
[35] M. Schütz, D. Usvyat, M. Lorenz, C. Pisani, L. Maschio, S. Casassa, and M. Halo, *Accurate Condensed-Phase Quantum Chemistry* (CRC, 2010).
[36] R. A. Evarestov and V. P. Smirnov, *Site Symmetry in Crystals* (Springer, 1996).
[37] R. A. Évarestov and I. I. Tupitsyn, Phys. Solid State **44**, 1656–1670 (2002).
[38] S. Varga, M. Milko, and J. Noga, J. Chem. Phys. **124**, 034106 (2006).
[39] J. W. Mintmire and B. I. Dunlap, Phys. Rev. A **25**, 88–95 (1982).
[40] F. R. Manby and P. J. Knowles, Phys. Rev. Lett. **87**, 163001 (2001).
[41] F. R. Manby, P. J. Knowles, and A. W. Lloyd, J. Chem. Phys. **115**, 9144 (2001).
[42] L. Maschio and D. Usvyat, Phys. Rev. B **78**, 073102 (2008).

[43]F. E. Harris, *Theoretical Chemistry: Advances And Perspectives* (Academic, New York, 1975), Vol. 1, p. 147.
[44]P. P. Ewald, Ann. Phys. **369**, 253–287 (1921).
[45]R. Dovesi, R. Orlando, B. Civalleri, C. Roetti, V. R. Saunders, and C. M. Zicovich-Wilson, Z. Kristollgr. **220**, 571–573 (2005).
[46]C. Pisani, R. Dovesi, and C. Roetti, *Hartree-Fock Ab Initio Treatment of Crystalline Solids*, Lecture Notes in Chemistry Vol. 48 (Springer-Verlag, Berlin, 1988).
[47]B. I. Dunlap, J. W. D. Connolly, and J. R. Sabin, J. Chem. Phys. **71**, 3396 (1979).
[48]B. I. Dunlap, Phys. Chem. Chem. Phys. **2**, 2113–2116 (2000).
[49]T. H. Dunning, J. Chem. Phys. **90**, 1007 (1989).
[50]B. P. Prascher, D. E. Woon, K. A. Peterson, T. H. Dunning, and A. K. Wilson, Theor. Chem. Acc. **128**, 69–82 (2011).
[51]R. Nada, J. B. Nicholas, M. I. McCarthy, and A. C. Hess, Int. J. Quantum Chem. **60**, 809–820 (1996).
[52]E. Voloshina, D. Usvyat, M. Schütz, Y. Dedkov, and B. Paulus, Phys. Chem. Chem. Phys. **13**, 12041–12047 (2011).
[53]See supplementary material at http://dx.doi.org/10.1063/1.4767775 for specification of the structural parameters, basis sets, and computational details.
[54]F. Weigend, M. Häser, H. Patzelt, and R. Ahlrichs, Chem. Phys. Lett. **294**, 143–152 (1998).
[55]C. Pisani, M. Schütz, S. Casassa, D. Usvyat, L. Maschio, M. Lorenz, and A. Erba, Phys. Chem. Chem. Phys. **14**, 7615–7628 (2012).
[56]D. Usvyat, B. Civalleri, L. Maschio, R. Dovesi, C. Pisani, and M. Schütz, J. Chem. Phys. **134**, 214105 (2011).
[57]W. Hanke and L. J. Sham, Phys. Rev. B **12**, 4501–4511 (1975).
[58]I. Souza, N. Marzari, and D. Vanderbilt, Phys. Rev. B **65**, 035109 (2001).
[59]U. Birkenheuer and D. Izotov, Phys. Rev. B **71**, 125116 (2005).
[60]R. J. Cave, *Modern Electronic Structure Theory and Applications in Organic Chemistry* (World Scientific, Singapore, 1997).
[61]S. Schmitt-Rink, D. S. Chemla, and D. A. B. Miller, Phys. Rev. B **32**, 6601–6609 (1985).
[62]A. Grüneis, M. Marsman, and G. Kresse, J. Chem. Phys. **133**, 074107 (2010).
[63]A. Schafer, H. Horn, and R. Ahlrichs, J. Chem. Phys. **97**, 2571 (1992).
[64]R. A. Kink, M. F. Kink, T. A. Soovik, V. G. Stankevich, A. V. Zabelin, N. Yu. Svechnikov, A. A. Kolmakov, S. O. Cholakh, V. A. Pustovarov, and A. N. Poliyenko, Nucl. Instrum. Methods Phys. Res. A **261**, 138–139 (1987).
[65]V. G. Plekhanov, Rep. Prog. Phys. **61**, 1045 (1998).
[66]K. Kobayashi, J. Phys. Chem. **87**, 4317–4321 (1983).
[67]O. Madelung, *Semiconductors - Basic Data*, 2nd ed. (Springer, 1996).
[68]P. Y. Yu and M. Cardona, *Fundamentals of Semiconductors*, 4th ed. (Springer, 2010).
[69]R. C. Whited, C. J. Flaten, and W. C. Walker, Solid State Commun. **13**, 1903–1905 (1973).
[70]G. H. Reiling and E. B. Hensley, Phys. Rev. **112**, 1106–1111 (1958).
[71]D. M. Roessler and W. C. Walker, J. Phys. Chem. Solids **28**, 1507–1515 (1967).
[72]M. Piacentini, D. W. Lynch, and C. G. Olson, Phys. Rev. B **13**, 5530–5543 (1976).
[73]O. Madelung, *Semiconductors: Data Handbook*, 3rd ed. (Springer, 2004).
[74]M. Head-Gordon, R. J. Ricoa, M. Oumia, and T. J. Leeb, Chem. Phys. Lett. **219**, 21–29 (1994).
[75]O. Christiansen, H. Koch, and P. Jørgensen, Chem. Phys. Lett. **243**, 409–418 (1995).
[76]C. Hättig and F. Weigend, J. Chem. Phys. **113**, 5154 (2000).
[77]D. Kats and M. Schütz, J. Chem. Phys. **131**, 124117 (2009).
[78]H. Stoll and A. Savin, *Density Functional Methods in Physics* (Plenum, New York, 1985).